ORNL/NRC/LTR-99/7

Contract Program or Project Title:	International Pressure Vessel Technology Cooperative Program
Subject of this Document:	NESC-II Pretest Thermal and Fracture Mechanics Analysis
Type of Document:	Letter Report
Authors:	B. R. Bass P. T. Williams
Date of Document:	March 1999
Responsible NRC Individual and NRC Office or Division	C. G. Santos (301) 415-6004 Division of Engineering Technology, U. S. Nuclear Regulatory Commission

Prepared for the
U.S. Nuclear Regulatory Commission
Washington, D.C. 20555-0001
Under Interagency Agreement DOE 1886-N663-1W
NRC JCN W6631

OAK RIDGE NATIONAL LABORATORY
Oak Ridge, Tennessee 37831-8056
managed by
LOCKHEED MARTIN ENERGY RESEARCH CORP.
for the
U. S. DEPARTMENT OF ENERGY
under Contract No. DE-AC05-96OR22464

ORNL/NRC/LTR-99/7

NESC-II Pretest Thermal and Fracture Mechanics Analysis

B. R. Bass and P. T. Williams

Oak Ridge National Laboratory

Oak Ridge, Tennessee

Manuscript Completed - February 1999
Date Published - March 1999

Prepared for the
U.S. Nuclear Regulatory Commission
Washington, D.C. 20555-0001
Under Interagency Agreement DOE 1886-N663-1W
NRC JCN W6631

OAK RIDGE NATIONAL LABORATORY
Oak Ridge, Tennessee 37831-8056
managed by
LOCKHEED MARTIN ENERGY RESEARCH CORP.
for the
U. S. DEPARTMENT OF ENERGY
under Contract No. DE-AC05-96OR22464

OAK RIDGE NATIONAL LABORATORY
MANAGED BY LOCKHEED MARTIN ENERGY RESEARCH CORPORATION
FOR THE U.S. DEPARTMENT OF ENERGY

NESC-II Pretest Thermal and Fracture Mechanics Analysis[1]

B. R. Bass and P. T. Williams
Oak Ridge National Laboratory
Oak Ridge, Tennessee USA

[1] Research Sponsored by the Office of Nuclear Regulatory Research, U.S. Nuclear Regulatory Commission under Interagency Agreement 1886-N663-1W with the U.S. Department of Energy under Contract DE-AC05-96OR22464 with Lockheed Martin Energy Research Corp. This manuscript has been authored by a contractor of the U.S. Government No. DE-AC05-96OR22464. Accordingly, the U.S. Government retains a nonexclusive, royalty-free license to publish or reproduce the published form of this contribution, or allow others to do so, for U.S. Government purposes.

INTRODUCTION

A pretest thermal and fracture mechanics stress analysis of the proposed NESC-II pressurized thermal shock (PTS) test, to be carried out at MPA-University of Stuttgart, Germany, has been performed based on the description of the test specimen and test conditions supplied in NESC-II TG3 Problem Definition Document as revised on 19 February 1999 [1]. The purpose of these pretest analyses is to make an assessment of the revised transient description with its new initial temperature condition of 250 °C. The issue to be addressed is whether the proposed transient will produce the desired cleavage initiation and arrest in terms of a "best estimate" analysis. The results of the ORNL pretest analyses along with recommendations are presented in this report.

PROBLEM DEFINITION AND INPUT DATA

CYLINDER GEOMETRY

Figure 1 gives a description of the cylinder geometry. The cylinder has an inner radius of 202.5 mm with a wall thickness of 190 mm including an 8 mm thick cladding on the inner surface. The 1/2 length of the cylinder measured from the symmetry plane is 580 mm with the cladding extending from the symmetry plane for a distance of 100 mm. Within this 100 mm, the cylinder is assumed to consist of two (2) materials: stainless steel *cladding* and *base* (17 MoV 8 4). Beyond the 100 mm test section, the material is assumed to be a single material designated as *Rest.*

DEFECT GEOMETRY

For the purposes of this analysis, the defect is assumed to be an 8 mm deep circumferential subclad flaw with uniform depth around the circumference of the cylinder.

THERMOPHYSICAL PROPERTIES

Reference [1] provides thermophysical properties for two materials: *base* and *cladding*. The *Rest* material is assumed to have the same thermophysical properties as the base.

Table 1. Thermophysical Properties

Property	Base Material	Cladding
Density (kg/m^3)	7806	7794
Thermal Expansion [$^{-1}$°C]	12.3×10^{-6}	16.5×10^{-6}
Thermal Conductivity [W/m-K]	47.4	17.9
Specific Heat [J/kg-K]	494	529

MECHANICAL PROPERTIES

Young's Modulus, *E*, is given in Ref. [1] as a function of temperature from 20 °C ≤ T ≤ 700°C for the *base*, *cladding* and *rest* materials. Poisson's ratio is assumed constant at 0.3 for all materials.

Table 2. Elastic Properties

Base (17 MoV 84)		Cladding		Rest	
Temp. (°C)	*E* (MPa)	Temp. (°C)	*E* (MPa)	Temp. (°C)	*E* (MPa)
20	214500	20	211180	20	210000
50	206900	50	211180	160	200000
100	207600	100	212670	220	194200
150	210100	150	207450	260	190300
200-700	213200	200	200580	320-700	184400
		250	195390		
		300	188530		
		350-700	185660		

True stress vs plastic strain data were provided in Ref. [1] as a function of temperature from 20 °C up to 700 °C for the *base* and *cladding* materials. The *Rest* material was assumed to have the same elastic-plastic properties as the *base* material.

FRACTURE PROPERTIES

Fracture toughness data for the *base* 17 MoV 8 4 material were provided in Table 4 of Ref. [1]. The specimens were designated with three groupings: NP1-AA, NP1-HA, and NT3-HA.

LOADINGS

MECHANICAL LOADING

Internal Pressure: 300 bar (30 MPa) constant over time
Axial Load: 40 MN, constant over time

THERMAL LOADING

The initial conditions consisted of a specified inner surface temperature of 250 °C and an outer surface temperature of 280 °C. The applied thermal loading during the thermal shock transient was given in Ref. [1] in terms of time-dependent Robin boundary conditions simulating the forced convection heat transfer of the fluid spraying on the inner surface of the cylinder and natural convection to the ambient on the outer surface.

Table 3. Inner Surface Thermal Boundary Conditions

Time min. (sec)	Fluid Temperature °C	Time min. (sec)	Film Coefficient kW/m^2-°C
0	250	0	0
0.175 (10.5)	250	1.125 (67.5)	13.5
0.325 (19.5)	200	1.4 (84)	15
0.55 (33.0)	90	2.125 (127.5)	16.6
0.775 (46.5)	45	12 (720)	16.6
1.3 (78.0)	23	27 (1620)	14.8
45.0 (2700)	23	45 (2700)	14.8

Table 4. Outer Surface Thermal Boundary Conditions

Time min. (sec)	Fluid Temperature °C	Time min. (sec)	Film Coefficient kW/m^2-°C
0	280	0	0.1
10 (600)	280	45 (2700)	0.1
20 (1200)	280		
45 (2700)	150		

FINITE ELEMENT MODEL

An axisymmetric finite element model was constructed using the MSC Patran mesh generation code as shown in Fig. 1. The ABAQUS Standard 5.8 (Ref. [2]) model consisted of 2250 nodes and 701 8-node isoparametric elements (ABAQUS element type CAX8R with reduced integration). The lower boundary is a reflective symmetry plane in which the flaw is embedded using a “keyhole” type focused meshing for the crack tip. Time-dependent thermal boundary conditions are applied to the inner and outer cylinder surfaces with the symmetry and upper planes treated as adiabatic. The internal pressure and axial loading are both applied as constant distributed loads along their respective surfaces. The axial load (assumed to be the total applied axial load including the pressure-induced longitudinal meridional stress, also known as the “blow-off” load) was converted into an equivalent negative pressure and applied to a layer of elastic elements located at the upper end of the model. The thermal and mechanical loads were treated as uncoupled loadings on the same mesh layout, allowing the thermal transient to be run first with the temperature distributions being transferred directly to the stress analysis run as nodal input data read from the ABAQUS thermal results file. The stress analysis applied the mechanical loading incrementally in the first step with the flaw open at the steady-state initial temperature condition (ignoring residual stresses). Subsequent static steps applied the thermal shock incrementally over the time of the transient. The analysis used a small-strain nonlinear elastic-plastic constitutive formulation for all materials, and *J*-integrals were calculated throughout the transient.

RESULTS AND DISCUSSION

Temperature profiles through the thickness of the cylinder are shown in Fig. 2 for selected times in the transient, and the crack tip temperature history is given in Fig. 3. The resulting *J*-integral history is shown in Fig. 4 and converted to an applied K_I in Fig. 5 by the plane strain formula

$$K_J = \sqrt{\left(\frac{E}{1-\nu^2}\right) J} \tag{1}$$

The resulting loadpath is presented in Fig. 6 along with the toughness data given in Ref. [1] and the ASME K_{IC} and K_{IA} curves for an estimated FATT50 of 140 °C. These ASME curves from Ref. [3] are

$$K_{IC} = 36.5 + 3.084 \exp\left[0.036\ \left(T - FATT50 + 55.56\right)\ \right] \tag{2}$$

$$K_{IA} = 29.5 + 1.344 \exp\left[0.026\ \left(T - FATT50 + 88.89\right)\ \right] \tag{3}$$

with K_{IC} and K_{IA} in [MPa-m$^{1/2}$] and T in [°C]. In the context of Figs. 6 and 7, the term "loadpath" refers to the applied K_I versus temperature curve proceeding from right to left (decreasing temperature at the crack tip) as the PTS transient evolves over time (from left to right in Fig. 5).

In Fig. 7, the loadpath for an applied tensile load of 40 MN provides a relatively small window for initiation, i.e., the interval between the ASME K_{IC} curve and the peak K_I-value that marks the onset of warm-prestressing. In this region, the peak K_I-value does not quite reach the mean value curve for the small specimen data. Increasing the applied load by 10-20 MN significantly increases the crack driving force relative to the magnitude of the fracture toughness data. Figure 8 provides rough estimates of the cleavage crack extension for the various load levels. The assumption is made that the time interval for cleavage crack propagation is considerably less than the fundamental period of the system response. Static analyses will predict larger crack extensions and a higher required material toughness for crack arrest than would be predicted by a more accurate dynamic analysis. We roughly approximate the latter by maintaining K_I constant for a fast fracture event, based on prior ORNL dynamic analyses of cleavage events in an RPV. The difference in predicted extension between 40 and 60 MN is not large relative to the wall thickness. We have not yet evaluated the propensity for ductile tearing following cleavage arrest of the crack. The fracture mechanics results are tabulated in Tables 5 through 7.

CONCLUSIONS AND RECOMMENDATIONS

A pretest thermal and fracture mechanics stress analysis of the proposed NESC-II pressurized thermal shock (PTS) test has been carried out. The issue to be addressed was whether the proposed transient will produce the desired cleavage initiation and arrest in the test cylinder.

Based on our analyses, we recommend that the applied axial mechanical loading of the specimen be increased from the MPA-recommended 40 MN to approximately 50 to 60 MN to improve the probability of attaining a cleavage initiation event; however, we recognize that other considerations involving test planning and execution not addressed by this analysis may be the determining factors in making the final decision regarding test conditions. We, therefore, do not regard our recommendation to be essential and would support a final decision, based on other factors, to maintain the current loading condition.

REFERENCES

[1] L. Stumpfrock and N. Taylor, *Structural Analysis Problem Definition Document*, NESC-II TG3 DOC (98) 002, Rev. 1, NESC Structural Analysis Group (TG3), 19 February 1999.

[2] *ABAQUS Theory Manual, Version 5.8*, Hibbit, Karlson and Sorensen, Inc., Providence, RI, 1998

[3] *ASME Boiler and Pressure Vessel Code, Section XI: Rules for Inservice Inspection of Nuclear Power Plant Components,* 1998 Edition, American Society of Mechanical Engineers, New York, NY, July 1, 1998.

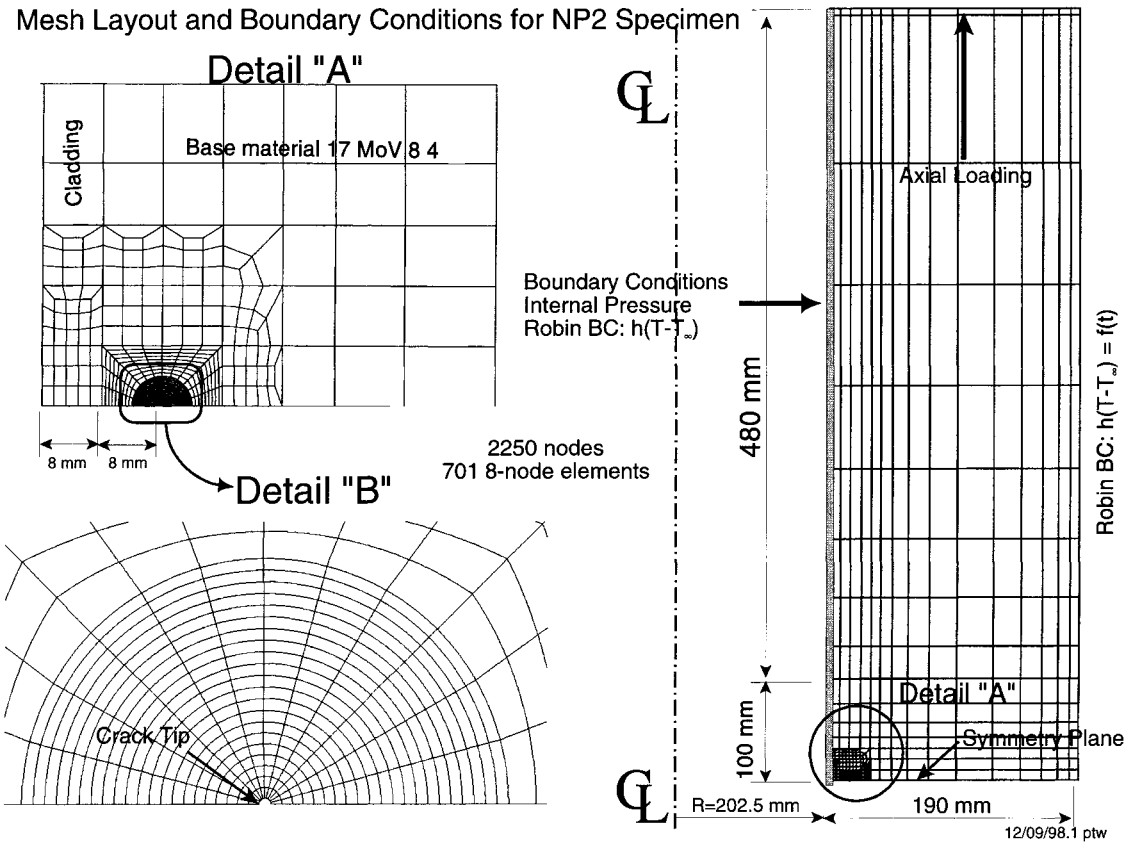

Fig. 1. Problem geometry: test cylinder and circumferential subclad defect.

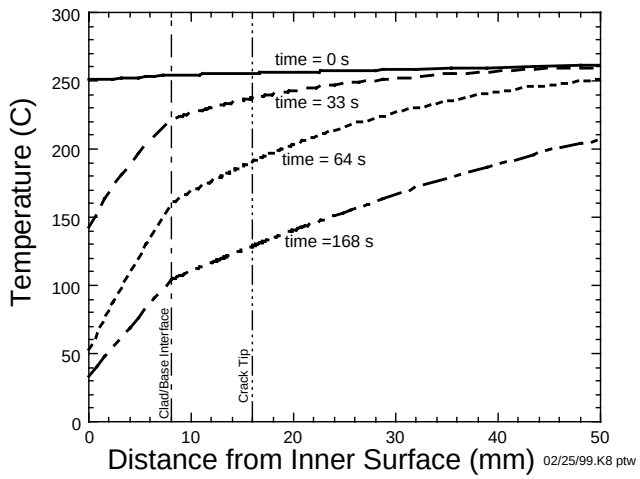

Fig. 2. Temperature profiles through the cylinder wall as a function of time.

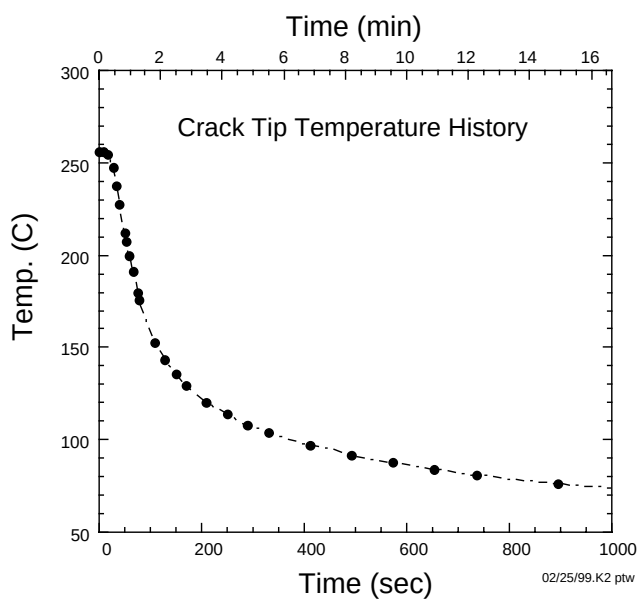

Fig. 3. Crack tip temperature history.

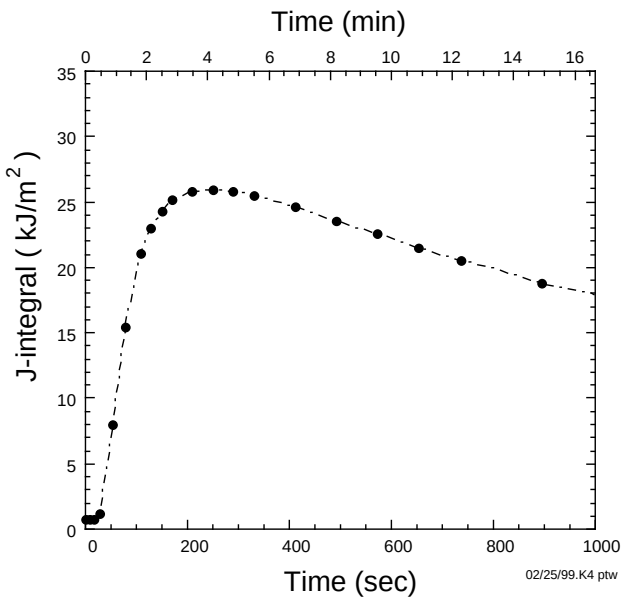

Fig. 4. *J*-integral time history.

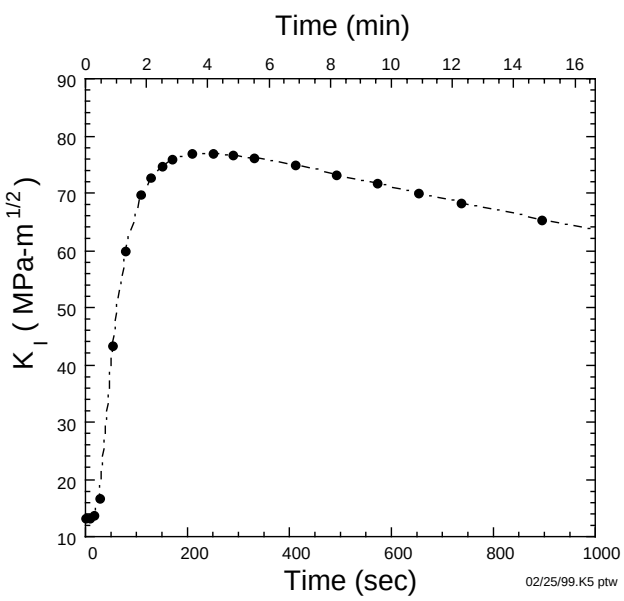

Fig. 5. Applied K_I history converted from *J*.

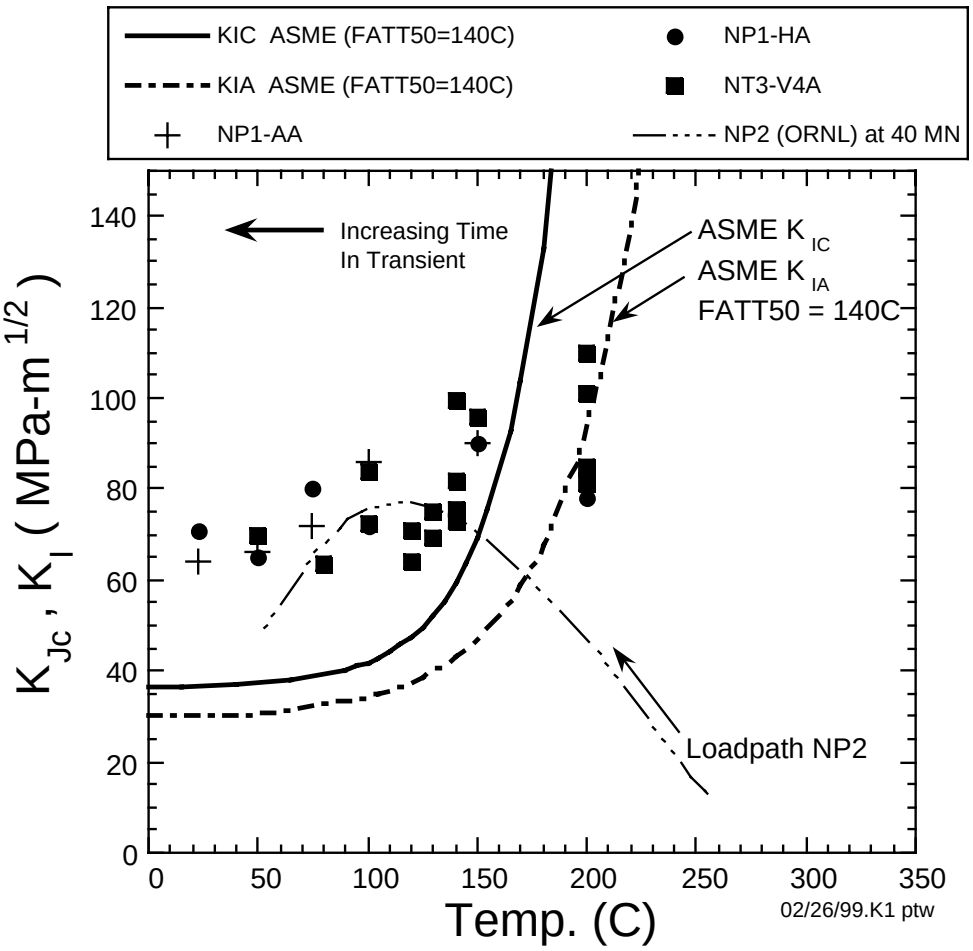

Fig. 6. Computed loadpath with toughness data and ASME K_{IC} and K_{IA} curves for FATT50 = 140 °C.

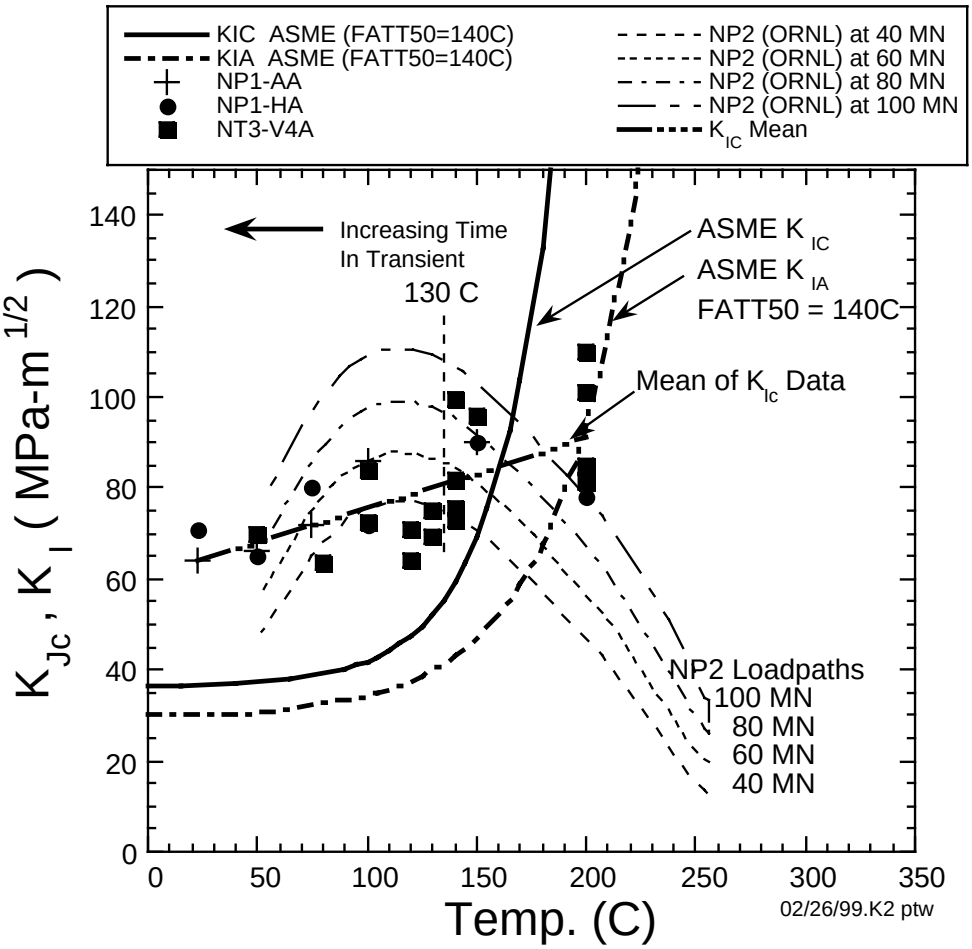

Fig. 7. Loadpaths for different applied axial mechanical loads.

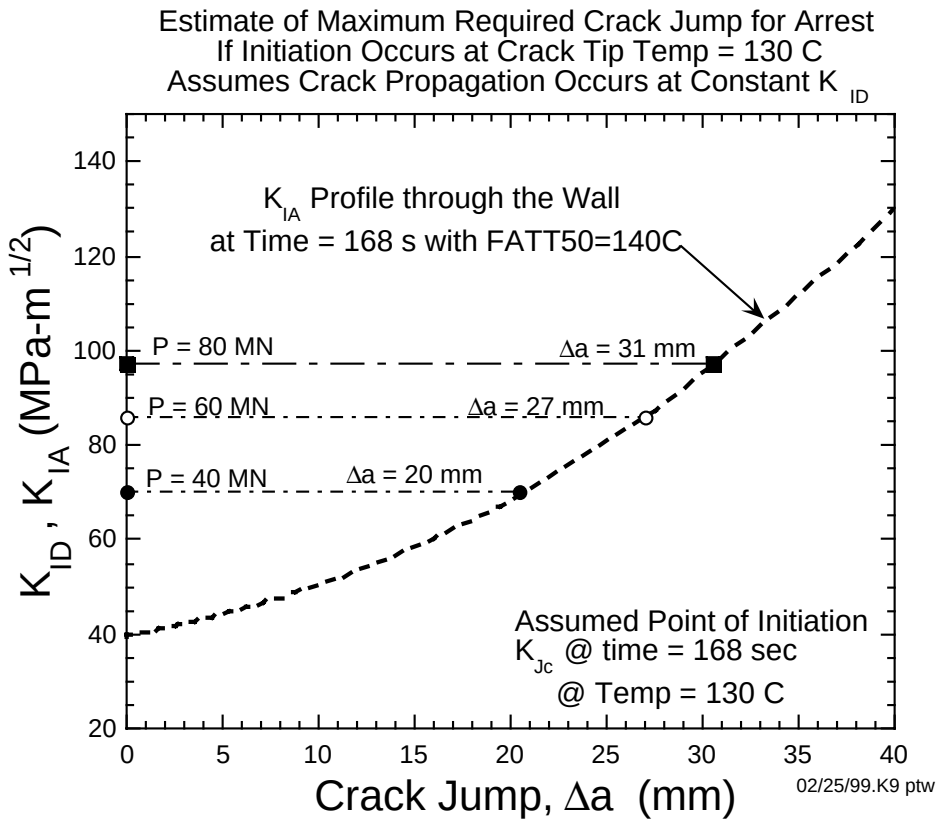

Fig. 8. Estimate of maximum crack jump required for arrest if initiation occurs at 130 °C.

Table 5. Results for 40 MN Applied Axial Mechanical Load

40 MN			
Time (s)	Temp. (°C)	K_J (MPa-m$^{1/2}$)	J (kJ/m^2)
0	255.690	13.258	0.750
0.51	255.690	13.259	0.750
1.02	255.690	13.259	0.750
8.19	255.840	13.158	0.739
16.4	254.360	13.745	0.806
27.6	247.760	16.717	1.193
52.8	207.370	43.258	7.987
78.1	175.650	59.900	15.424
108	152.750	69.697	21.023
129	143.160	72.848	23.03
149	135.620	74.774	24.313
169	129.500	75.971	25.137
209	120.570	76.887	25.804
250	113.700	77.036	25.944
290	108.230	76.789	25.807
331	103.750	76.304	25.505
412	97.086	74.901	24.604
492	91.880	73.302	23.584
573	87.632	71.629	22.532
654	84.044	69.959	21.503
735	80.934	68.330	20.52
895	75.928	65.342	18.773
1058	71.733	62.663	17.27
2188	52.896	48.568	10.376

Table 6. Results for 60 MN Applied Axial Mechanical Load

60 MN			
Time (s)	Temp. (°C)	K_J (MPa-m$^{1/2}$)	J (kJ/m^2)
0	255.690	19.783	1.671
0.51	255.690	19.784	1.671
1.02	255.690	19.784	1.671
8.19	255.840	19.683	1.654
16.4	254.360	20.269	1.753
27.6	247.760	23.577	2.373
52.8	207.370	52.845	11.920
78.1	175.650	70.071	21.106
108	152.750	80.216	27.848
129	143.160	83.485	30.246
149	135.620	85.493	31.783
169	129.500	86.732	32.764
209	120.570	87.693	33.567
250	113.70	87.868	33.753
290	108.230	87.615	33.597
331	103.750	87.118	33.246
412	97.086	85.671	32.188
492	91.880	84.018	30.983
573	87.632	82.284	29.734
654	84.044	80.549	28.506
735	80.934	78.854	27.328
895	75.928	75.737	25.221
1058	71.733	72.934	23.395
2188	52.896	57.996	14.796

Table 7. Results for 80 MN Applied Axial Mechanical Load

80 MN			
Time (s)	Temp. (°C)	K_J (MPa-m$^{1/2}$)	J (kJ/m^2)
0	255.690	26.381	2.971
0.51	255.690	26.382	2.971
1.02	255.690	26.382	2.971
8.19	255.840	26.281	2.948
16.4	254.360	26.894	3.087
27.6	247.760	31.703	4.290
52.8	207.370	63.075	16.981
59.13	199.440	67.429	19.409
65.45	191.510	71.700	21.996
74.94	179.620	78.214	26.266
78.1	175.650	80.391	27.782
108	152.750	90.905	35.764
129	143.160	94.340	38.623
149	135.620	96.477	40.475
169	129.500	97.782	41.644
209	120.570	98.807	42.614
250	113.700	99.001	42.848
290	108.230	98.744	42.674
331	103.750	98.229	42.267
412	97.086	96.723	41.029
492	91.880	94.998	39.610
573	87.632	93.183	38.133
654	84.044	91.364	36.674
735	80.934	89.583	35.270
895	75.928	86.300	32.747
1058	71.733	83.339	30.547
2188	52.896	67.380	19.971

Internal Distribution

1-5. B. R. Bass
6. K. W. Childs
7. T. L. Dickson
8. D. M. Hetrick
9. M. A. Kuliasha
10. W. J. McAfee
11. R. K. Nanstad
12. C. E. Pugh
13-17. P. T. Williams
18. Laboratory Records - RC

External Distribution

28. K. R. Wichman, EMCB/DE/NRR, U.S. Nuclear Regulatory Commission, Mailstop O7 D4, Washington, D.C. 20555-0001
29. E. M. Hackett, EMMEB/DET/RES, U.S. Nuclear Regulatory Commission, Mailstop T10 E10, Washington, D.C. 20555-0001
30. S. N. Malik, EMMEB/DET/RES, U.S. Nuclear Regulatory Commission, Mailstop T10 E10, Washington, D.C. 20555-0001
31. M. E. Mayfield, DET/RES, U.S. Nuclear Regulatory Commission, Mailstop T10 E10, Washington, D.C. 20555-0001
32-36. C. G. Santos, EMMEB/DET/RES, U.S. Nuclear Regulatory Commission, Mailstop T10 E10, Washington, D.C. 20555-0001
37. R. L. Tregoning, Fatigue and Fracture Branch, Carderock Division, Naval Surface Warfare Center, 9500 McArthur Blvd., West Bethesda, MD 20817-5700.
38. J. A. Joyce, U.S. Naval Academy, Mechanical Engineering Department, MS-11C, 590 Hollway Road, Annapolis, MD 21402
39. R. H. Dodds, Jr., 3140 Newmark Laboratory, 205 North Matthews, Urbana, Illinois 61801